INSTITUTE FOR FUSION STUDIES

DOE/ET-53088-523 IFSR #523

Drift Wave Vortices in Nonuniform Plasmas and Sheared Magnetic Fields

X.N. SU, W. HORTON, and P.J. MORRISON
Department of Physics and Institute for Fusion Studies
The University of Texas at Austin
Austin, Texas 78712

November 1991

THE UNIVERSITY OF TEXAS

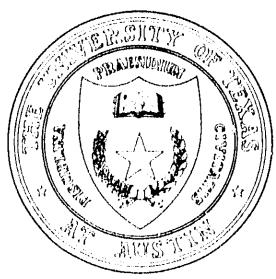

AUSTIN

DISCLAIMER

Drift Wave Vortices in Nonuniform Plasmas with Sheared Magnetic Fields

X.N. Su, W. Horton, and P.J. Morrison
Department of Physics and
Institute for Fusion Studies
The University of Texas at Austin
Austin, Texas 78712

DOE/ET/53088--523

DE92 006879

Abstract

Nonlinear coherent structures governed by the coupled drift wave-ion acoustic mode equations in nonuniform plasmas with sheared magnetic fields are studied analytically and numerically. A solitary vortex equation that includes the effects of density and temperature gradients, and magnetic shear is derived and analyzed. The analytic and numerical studies show that for a plasma in a sheared magnetic field, even without the temperature and drift velocity gradients, solitary vortex solutions are possible; however, these solutions are not exponentially localized due to the presence of a non-structurally stable perturbative tail that connects to the core of the vortex. The new coherent vortex structures are dipole-like in their symmetry, but are not the modons of Larichev and Reznik. In the presence of a small temperature or drift velocity gradient, the new shear-induced dipole can not survive and will separate into monopoles, like the case of the modon in a sheared drift velocity as studied in Su *et al.* [Phys. Fluids B 3, 921 (1991)]. The solitary solutions are found from the nonlinear eigenvalue problem for the effective potential in a quasi-one-dimensional approximation. The numerical simulations are performed in 2-D with the coupled vorticity and parallel mass flow equations.

I. Introduction

Since the solitary dipole vortex solutions or modons were found[1] for the Hasegawa-Mima[2] (H-M) drift wave equation in a uniform plasma, numerous works[3-8] have concerned solitary vortex solutions in nonuniform plasmas. Petviashvili first suggested that if the H-M equation is modified by including the effect of the electron temperature gradient, one can derive solitary monopole vortex solutions. The derivation of the original Petviashvili model,[3] however, has been shown to be incomplete recently by several authors.[5-8] In particular, the full analysis shows that non-locality of the linear wave operator must be retained simultaneously with the KdV-type nonlinearity introduced by Petviashvili, in order to preserve the conservation of potential vorticity. The authors have shown that for a plasma with constant drift velocity v_d, there exist no monopole vortex solutions, no matter what the temperature profile, $T(x)$; but monopole solutions can exist if the drift velocity is not constant $v_d(x)$. In recent work[8] we have considered a fully nonlinear model with a Boltzmann density distribution and have concluded that the monopole-like vortices can exist if the temperature and drift velocity are not constant. Such monopole-like vortices are not exponentially localized soliton-like monopoles since the inhomogeneity also causes energy leakage from the vortex core through radiative tails. This leakage will be negligible if the strength of the inhomogeneity $\alpha = |T'/T^2 - v'_{d0}/u|$ and size of the vortex $1/k_0$ (where $k_0 \equiv \sqrt{1 - v_{d0}/u}$) satisfy $\alpha \ll k_0^3$.

In all previous work,[3-8] the spatial dependence of $k_{||}$ is ignored, and consequently the effects of magnetic shear are systematically eliminated. The present paper extends previous work[8] by taking into account the nonlinear coupling of vorticity to the magnetic shear induced parallel ion motion. Here a model that includes not only the temperature and density gradients, but also the effect of magnetic shear is developed and analyzed. Analytically

we consider a quasi-one-dimensional model for the finite amplitude coherent structures that exhibits a nonlinear localization mechanism. With this model we are able to show that when the effect of magnetic shear is included in the drift wave equation, even without the gradient of drift velocity, the effective potential becomes a nonlinear trapping potential and, therefore, there exist solitary solutions. The solutions are shown to be dipole-like solitary waves. However, they are different from the well-known modons which are exact solutions of the H-M equation. Due to the coupling of drift waves to ion acoustic waves, the solitary structures, like those induced by nonconstant drift velocity in a shearless field,[8] are not exponentially localized soliton-like solutions; instead they have oscillating tails which connect to the cores of the vortices. We also use 2-D magneto-hydrodynamic type of numerical code to simulate the coupled vorticity and parallel velocity fields. The numerical results are consistent with the analytic results obtained from the quasi-one-dimensional model.

The article is organized as follows. In Sec. II the model equations are derived and the conservation laws are presented. In Sec. III the model equations are analyzed. The numerical results are presented and discussed in Sec. IV. Finally, summary and conclusions are given in Sec. V.

II. Model Equations and Conservation Laws

We consider a plasma of cold ions and massless electrons in a sheared external magnetic field $\mathbf{B} = B_0(\hat{\mathbf{z}} + \mathcal{S}(x)/L_s\hat{\mathbf{y}}) = B_0\hat{\mathbf{b}}$. The dissipationless equation of motion and the continuity equation for the ions are

$$\frac{d\mathbf{v}}{dt} = -\frac{e}{m_i}\nabla\Phi + \mathbf{v}\times\mathbf{\Omega}\,, \tag{1}$$

$$\frac{\partial n}{\partial t} + \nabla\cdot(n\mathbf{v}) = 0\,, \tag{2}$$

where $d/dt = \partial/\partial t + \mathbf{v}\cdot\nabla$, and $\mathbf{\Omega} = e\mathbf{B}/m_ic = \omega_{ci}\hat{\mathbf{b}}$ is the ion cyclotron frequency. Upon taking the curl of Eq. (1) and combining with Eq. (2), one can derive the inhomogeneous

Ertel's theorem,

$$\frac{d}{dt}\left(\frac{\boldsymbol{\Omega}+\boldsymbol{\omega}}{n}\right)=\left(\frac{\boldsymbol{\Omega}+\boldsymbol{\omega}}{n}\right)\cdot\nabla\mathbf{v}\ ,$$

where $\boldsymbol{\omega}=\nabla\times\mathbf{v}$. (3)

Introducing the ordering,

$$\epsilon_t\equiv\frac{1}{\omega_{ci}}\frac{\partial}{\partial t}\sim\frac{\mathbf{v}\cdot\nabla}{\omega_{ci}}\sim\frac{\nabla_{\|}v_{\|}}{\omega_{ci}}\ll 1\ ,$$

we obtain from Eq. (1) to lowest order in ϵ_t

$$\mathbf{v}=\mathbf{v}_{\perp}=(\frac{e}{m_i\omega_{ci}})\hat{\mathbf{z}}\times\nabla\Phi$$

$$\boldsymbol{\omega}=\omega_{ci}\frac{\rho_s^2}{T_e}\nabla_{\perp}^2(e\Phi)\hat{\mathbf{z}}$$

and the convective derivative becomes

$$\frac{d}{dt}=\frac{\partial}{\partial t}+\mathbf{v}_{\perp}\cdot\nabla=\frac{\partial}{\partial t}+\omega_{ci}\frac{\rho_s^2}{T_e}[e\Phi\ ,\ ]\ ,$$

where $\rho_s=c_s/\omega_{ci}$ and $c_s=(T_e(x)/m_i)^{1/2}$. Now we define $T(x)=T_e(x)/T_0$ (where T_0 is a constant), $r_n^{-1}=-d\ell n\, n_0/dx$, $\epsilon_n=\rho_{s0}/r_n$, $\rho_{s0}=c_{s0}/\omega_{ci}=(T_0/m_i)^{1/2}/\omega_{ci}$ and the magnetic shear strength $S(x)=(r_n/L_s)\mathcal{S}(x)$. The parallel component of the vorticity equation from Eq. (3) can now be written as

$$\frac{\partial}{\partial t}\ell n\left(\frac{1+\epsilon_n\nabla_{\perp}^2\varphi}{n}\right)+\left[\varphi\ ,\quad \ell n\left(\frac{1+\epsilon_n\nabla_{\perp}^2\varphi}{n}\right)\right]=\left(\frac{\partial}{\partial z}+S(x)\frac{\partial}{\partial y}\right)\epsilon_n v_{\|}\ , \tag{4}$$

and the parallel component of the momentum equation from Eq. (1) is

$$\frac{\partial v_{\|}}{\partial t}+\left[\varphi\ ,\quad v_{\|}\right]=-\left(\frac{\partial}{\partial z}+S(x)\frac{\partial}{\partial y}\right)\varphi\ . \tag{5}$$

For the massless electrons, we assume the Boltzmann distribution

$$n=n_0(x)\exp\left(\frac{e\Phi}{T_e}\right)=n_0(x)\exp\left(\frac{\epsilon_n\varphi}{T}\right)\ . \tag{6}$$

In writing Eqs. (4)–(6), we have used the following scaling transformations to dimensionless variables: $x, y \rightarrow x/\rho_{s0},\ y/\rho_{s0}\ ;\ z \rightarrow z/r_n\ ;\ t \rightarrow (c_{s0}/r_n)t\ ;\ v_{\|} \rightarrow (r_n/\rho_{s0}c_{s0})v_{\|}\ ;\ \varphi \rightarrow (r_n e/\rho_{s0}T_0)\Phi$.

Upon substitution Eq. (6) into Eq. (4) and considering the ordering

$$\frac{r_n}{c_{s0}}\frac{\partial}{\partial t} \sim \rho_{s0}^2\nabla_{\perp}^2 \sim r_n\nabla_{\|} \sim \frac{e\Phi}{T} \sim \frac{v}{c_{s0}} \sim \frac{\rho_{s0}}{r_n} \equiv \epsilon_n \sim \epsilon\ , \tag{7}$$

we can rewrite Eq. (4) to order ϵ and ϵ^2 as

$$\left(\frac{1}{T} - \nabla^2\right)\frac{\partial\varphi}{\partial t} + v_d\frac{\partial\varphi}{\partial y} - \kappa_T\varphi\frac{\partial\varphi}{\partial y} - \left[\varphi,\ \nabla_{\perp}^2\varphi\right] = -\left(\frac{\partial}{\partial z} + S(x)\frac{\partial}{\partial y}\right)v_{\|}\ , \tag{8}$$

where $v_d(x) = -d\ell nn_0/dx \sim \mathcal{O}(1)$ and $\kappa_T(x) = -(1/T)d\ell nT/dx \sim \mathcal{O}(\epsilon)$.

Now the conservation law for mass is evident by rewriting Eq. (8) as

$$\frac{\partial}{\partial t}\left(\frac{\varphi}{T(x)}\right) + \boldsymbol{\nabla}\cdot\left[-\frac{\partial\nabla\varphi}{\partial t} + \left(v_d(x)\varphi - \frac{\kappa_T(x)\varphi^2}{2}\right)\hat{\mathbf{y}} + (\boldsymbol{\nabla}\varphi\times\hat{\mathbf{z}})\nabla^2\varphi + v_{\|}\hat{\mathbf{b}}\right] = 0\ , \tag{9}$$

and momentum conservation by rewriting Eq. (5) as

$$\frac{\partial}{\partial t}v_{\|} + \boldsymbol{\nabla}\cdot\left[(\boldsymbol{\nabla}\varphi\times\hat{\mathbf{z}})v_{\|} + \varphi\hat{\mathbf{b}}\right] = 0\ . \tag{10}$$

The conservation law for energy can be obtained by multiplying Eq. (5) by $v_{\|}$ and Eq. (8) by φ and then combining the two equations to get

$$\frac{\partial\mathcal{E}}{\partial t} + \boldsymbol{\nabla}\cdot\left[\left(\frac{v_d(x)}{2}\varphi^2 - \frac{\kappa_T(x)}{3}\varphi^3\right)\hat{\mathbf{y}} - \varphi\nabla\frac{\partial\varphi}{\partial t} - \nabla^2\varphi\left(\hat{\mathbf{z}}\times\nabla\frac{\varphi^2}{2}\right) + (\varphi v_{\|})\hat{\mathbf{b}}\right] = 0\ , \tag{11}$$

where the energy density $\mathcal{E}$ is defined as

$$\mathcal{E}(x,y,t) = \frac{1}{2}\left[\frac{\varphi^2}{T(x)} + (\nabla\varphi)^2 + v_{\|}^2\right]\ .$$

Therefore, Eqs. (9), (10) and (11) show that the dynamical system conserves mass, momentum and energy to the second order in ϵ.

Equation (4) describes the advection of the generalized potential vorticity and its change caused by parallel compression $\nabla_{\|}v_{\|}$. The compression from the parallel motion elimiates the conservation of potential enstrophy, defined as $U = \int(\nabla_{\perp}\varphi)^2 + (\nabla_{\perp}^2\varphi)^2 dx\,dy$.

However, the generalized cross helicity appears as constant of motion. To systematically construct the invariants, the so-called Casimir noncanonical Hamiltonian structure is developed in the Appendix. Here we observe that if we introduce the antiderivative of the shear $\sigma(x) = \int^x S(x')dx'$ such that $[\sigma(x),\ v_{||}] = S(x)\partial v_{||}/\partial y$ and the potential vorticity $q = \nabla^2\varphi - \varphi/T(x) - \ell n n_0(x)$, then it is straightforward to show that the conserved helicity is

$$h = \int q\left(v_{||} - \sigma(x)\right) dxdydz\ . \tag{12}$$

A generalization of this invariant in the case where z-dependence is neglected is given in the Appendix.

III. Travelling Wave Equation and Solitary Wave Solutions

Now we look for travelling wave solutions of Eqs. (4) and (5) by assuming $\varphi = \varphi(x, y-ut)$ and $v_{||} = v_{||}(x, y-ut)$. Equations (4) and (5) become

$$-u\frac{\partial}{\partial y}\ell n\left(\frac{1+\epsilon_n\nabla^2\varphi}{n}\right) + \left[\varphi,\quad \ell n\left(\frac{1+\epsilon_n\nabla^2\varphi}{n}\right)\right] = \epsilon_n S(x)\frac{\partial v_{||}}{\partial y}\ , \tag{13}$$

$$-u\frac{\partial v_{||}}{\partial y} + \left[\varphi\,, v_{||}\right] = -S(x)\frac{\partial\varphi}{\partial y}\ . \tag{14}$$

Equation (14) gives

$$\left[\varphi - ux\,,\ v_{||} + \sum_{n=1}^{\infty}(-1)^n\frac{d^{(n-1)}S(x)/dx^{(n-1)}}{n!u^n}\varphi^n\right] = 0\ , \tag{15}$$

which has the general solution

$$v_{||} - \frac{S_1 x}{u}\varphi + \frac{S_1}{2u^2}\varphi^2 = G(\varphi - ux)\ , \tag{16}$$

where G is an arbitrary function of its argument. In writing Eq. (16), we have expanded $S(x) = S_0 + S_1 x + S_2 x^2 + \ldots$ with $S_0 = 0$ and noticed that the higher order derivatives of $S(x)$ are significantly smaller than the first order derivative for the magnetic shear problem.

For localized solutions $\varphi \to 0$ as $r \to \infty$ and we assume the boundary condition $v_{||} \to v_\infty$ = constant as $r \to \infty$. Assuming $G(\infty) = v_\infty$, $v_{||}$ can be written as

$$v_{||} = \frac{S_1 x}{u}\varphi - \frac{S_1}{2u^2}\varphi^2 + v_\infty \ , \tag{17}$$

where we see that the magnetic shear introduces an important nonlinearity into the dependence of $v_{||}$ on φ.

Substituting Eq. (17) into Eq. (13), we obtain another condition

$$\left[\varphi - ux \ , \ell n\left(\frac{1+\epsilon_n\nabla^2\varphi}{n}\right) + \frac{\epsilon_n S_1^2 x^2}{u^2}\varphi - \frac{3\epsilon_n S_1^2 x}{2u^3}\varphi^2 + \frac{\epsilon_n S_1^2}{2u^4}\varphi^3\right] = 0 \ . \tag{18}$$

which has the general solution

$$\ell n\left(1+\epsilon_n\nabla^2\varphi\right) - \ell n\, n_0 - \frac{\epsilon_n\varphi}{T(x)} + \frac{\epsilon_n S_1^2 x^2}{u^2}\varphi - \frac{3\epsilon_n S_1^2 x}{2u^3}\varphi^2 + \frac{\epsilon_n S_1^2}{2u^4}\varphi^3 = F(\varphi - ux) \ , \tag{19}$$

where we have assumed quasi-neutrality with the electrons obeying the Boltzmann distribution of Eq. (6). Again we see that the presence of magnetic shear introduces important strong nonlinearities into the system.

To insure localization for φ we select

$$F(\varphi - ux) = -\ell n\, n_0\left(\frac{ux-\varphi}{u}\right) \ . \tag{20}$$

For a simple exponential density profile, $n_0(x) = \exp(-\epsilon_n x)$, and constant temperature ($T = 1$), Eq. (19) with Eq. (20) becomes

$$\epsilon_n\nabla^2\varphi = \exp\left[\epsilon_n\left(1-\frac{v_d}{u}\right)\varphi - \epsilon_n S_1^2\left(\frac{x^2}{u^2}\varphi - \frac{3x}{2u^3}\varphi^2 + \frac{\varphi^3}{2u^4}\right)\right] - 1 \ , \tag{21}$$

where $v_d = 1$ follows from the choice of units.

Considering the quasi-one-dimensional case in which $\partial/\partial y \ll \partial/\partial x$ and introducing the new variables

$$k^2 = 1 - \frac{1}{u} \ , \ x = \frac{t}{k} \ , \ \varphi = \frac{u}{k}\Psi \ , \ s^2 = \frac{S_1^2}{2u^2k^4} \ , \ \epsilon_0 = uk\epsilon_n \ ,$$

we obtain

$$\epsilon_0 \frac{\partial^2 \Psi}{\partial t^2} = \exp\left[\epsilon_0 \left(\Psi - s^2(2t^2\Psi - 3t\Psi^2 + \Psi^3)\right)\right] - 1 \ . \tag{22}$$

Here, note that for small k^2, corresponding to large coherent structures, the effective shear parameter s^2 is considerably enhanced over the original shear parameter S_1^2.

The boundary condition $\Psi(t \to \pm\infty) \to 0$ and the initial conditions $\Psi(t=0) = 0$ and $d\Psi(t=0)/dt = $ const. or $\Psi(t=0) = $ const. and $d\Psi(t=0)/dt = 0$ together with Eq. (22) define a nonlinear eigenvalue problem for the unknown constant values at $t = 0$.

In the new variables we can calculate the rotation rate[4] $\Omega_E = (c_s/r_n)k_y d\varphi/dx$ compared to the vortex frequency $\omega_{\rm lab} = (c_s/r_n)k_y u$ in the laboratory frame as $\Omega_E/\omega_{\rm lab} = d\Psi/dt$.

Equation (22) can be written in the form of the Hamiltonian equations for an imaginary particle with coordinate $q = \Psi$, time t, and momentum $p = \partial\Psi/\partial t$ in the effective potential

$$V_{\rm eff}(\Psi, t) = -\frac{1}{\epsilon_0}\int^{\Psi} d\Psi \, \exp\left[\epsilon_0 \left(\Psi - s^2(2t^2\Psi - 3t\Psi^2 + \Psi^3)\right)\right] + \frac{\Psi}{\epsilon_0} \ , \tag{23}$$

For $u \sim v_d = 1$, $\epsilon_0 \sim \epsilon_n^2 \ll 1$ and the effective potential reduces to

$$V_{\rm eff}(\Psi, t) \approx -\left[\frac{\Psi^2}{2} - s^2\left(t^2\Psi^2 - t\Psi^3 + \frac{\Psi^4}{4}\right)\right] \ . \tag{24}$$

Although for simplicity in Eq. (24) we have kept only the lowest order of $V_{\rm eff}$ in ϵ_0, it can easily be shown that this approximation does not change the shape of $v_{\rm eff}$.

The dynamical equations for a "particle" representing the system are

$$\dot{p} = -\frac{\partial}{\partial\Psi} V_{\rm eff}(\Psi, t) = \Psi - s^2(2t^2\Psi - 3t\Psi^2 + \Psi^3) \ , \tag{25}$$

$$\dot{\Psi} = p \ . \tag{26}$$

In order for Eq. (22) to have localized solutions, the effective potential must be a trapping potential. In the limit of $s \to 0$ the effective potential has the form $V_{\rm eff}(s=0) = \Psi - (1/\epsilon_0)e^{\epsilon_0\Psi}$ or to lowest order $V_{\rm eff}(s=0) \approx -(1/2)\Psi^2$, which is easily seen to not be a trapping potential. However, with existence of small shear s, the situation is changed entirely. To

realize this, one can examine the properties of $V_{\rm eff}$. The extremal points of the potential are given by

$$-\frac{\partial V_{\rm eff}}{\partial \Psi} = \Psi - s^2(2t^2\Psi - 3t\Psi^2 + \Psi^3) = 0$$

which yields $\Psi_{m1} = 0$, $\Psi_{m2} = (3/2)t - (1/2)\sqrt{t^2 + 4/s^2}$, and $\Psi_{m3} = (3/2)t + (1/2)\sqrt{t^2 + 4/s^2}$. The signs of second derivative $\partial^2 V_{\rm eff}/\partial \Psi^2$ at the extremal points determine the shape of the potential. Figure 1 is a sketch of the evolution of the effective potential with "time" t. Figure 2 displays corresponding phase space portraits showing the bifurcation of the origin from unstable to stable at $t = \sqrt{2}/2s$. It is evident that the effective potential has two wells when $t = 0$, indicated by I and II in Fig. 1. Well I moves to $\Psi = 0$ and disappears as $t \to \sqrt{2}/2s$ and then a new trapping Well III appears and stays at $\Psi = 0$ for $t > \sqrt{2}/2s$, while Well II moves towards $\Psi \to \infty$ as $t \to \infty$. For $t < 0$, Well II moves to $\Psi = 0$ and disappears as $t \to -\sqrt{2}/2s$ and a new trapping Well III appears and stays at $\Psi = 0$ for $t < -\sqrt{2}/2s$, while Well I moves towards $\Psi \to -\infty$ as $t \to -\infty$. Therefore only a "particle" eventually trapped in Well III corresponds to a solution satisfying the boundary conditions. The initial conditions determine if the "particle" will be eventually trapped in the Well III.

The presence of the trapping well indicates that the existence of magnetic shear changes the effective potential from nontrapping to trapping, and therefore creates the possibility of solitary wave solutions with finite amplitudes. However, the presence of magnetic shear also makes the solitary drift wave couple to the ion acoustic wave by changing the effective potential $V_{\rm eff}(\Psi, t)$ at the critical "time" $t_0 = \pm\sqrt{2}/2s$. The new trapping Well III that appears when $|t| > |t_0|$ actually is the potential well associated with the ion acoustic wave. The coupling between the solitary waves and the propagating ion acoustic waves leads to the formation of the oscillating tail emanating from the core of vortex. This tail gives rise to the dissipation of energy from the solitary wave core. Therefore, for a solitary vortex solution, the oscillating tail must be far away from the core of vortex, that is, $t_0 > 1$ or $x_0 > 1/k$, where $1/k$ is the size of the solitary vortex. This gives $s < \sqrt{2}/2$ or $S_1 < |u - v_d|$, which

is consistent with the condition for a modon with small damping given earlier by Meiss and Horton.[9]

Equations (24) and (25) are symmetric under the following transformations:

$$V_{\rm eff}(\Psi, t) \longrightarrow V_{\rm eff}(-\Psi, -t) \ ,$$

$$\Psi(t) \longrightarrow -\Psi(-t) \ . \tag{27}$$

These relations rule out the possibility of monopole solutions, since these are symmetric about $t = 0$. However, localized solutions in the form of dipoles are not ruled out. The shape of such a dipole is determined by the initial conditions $\Psi(t = 0) = 0$ and $d\Psi(t = 0)/dt =$ constant corresponding to the strength of the core electric field or $\mathbf{E} \times \mathbf{B}$ flow velocity. Numerical integration of Eq. (25) yieldes the spectrum of eigenvalues for the initial momentum $d\Psi(t = 0)/dt$ or equivalently $(1/u)d\varphi(x = 0)/dx$. Solutions are constructed by choosing the initial condition of zero coordinate and nonzero momentum, and then integrating beyond $t_0 = \pm\sqrt{2}/2s$ to determine if there is trapping as $t \rightarrow \pm\infty$ in the ion acoustic potential well. Physically the trapping implies the radiative tail at large t.

Figure 3 shows an example of a nonlinear trapping solution for $s = 0.06$. Clearly the trapping solutions of this form only occur for certain initial data , which depend on the shear parameter s. The magnitude of $d\Psi(t = 0)/dt$ and the initial amplitude Ψ_m of the vortex can be estimated with the help of Eq. (25). For small $t \leq t_m \sim \epsilon_0 < 1$, where t_m is the "time" at which Ψ assumes its maximum value or amplitude $\Psi_m \equiv \Psi(t = t_m)$ and $d\Psi(t = t_m)/dt = 0$, the second and third terms on the right side of Eq. (25) are much less than the first and fourth. Therefore for a nonlinear solitary solution, there must be a balance between the linear and nonlinear terms on Eq. (25), that is, $\Psi \sim s^2\Psi^3$. This gives the scaling law for amplitude of the vortex,

$$\Psi_m \sim \frac{1}{s} \qquad \text{or} \qquad \varphi_m \sim \frac{\sqrt{2}u^2k}{S_1} \ . \tag{28}$$

On the other hand, multiplying both sides of Eq. (25) by $d\Psi/dt$ and integrating in time from $t = 0$ to $t = t_m$, we can approximately get $\Psi'(0) \approx (s^2/2)\Psi_m^4 - \Psi_m^2$, where $\Psi'(0) \equiv d\Psi(t = 0)/dt$. Therefore the scaling law for the $\Psi'(0)$ is

$$\Psi'(0) \equiv \frac{d\Psi(t=0)}{dt} \sim \frac{1}{s} \qquad \text{or} \qquad \varphi'(0) \equiv \frac{d\varphi(x=0)}{dx} \sim \frac{\sqrt{2}u^2k^2}{S_1} \,. \tag{29}$$

A detailed study of the numerical spectrum yields the $\Psi'(0)$ vs. s curve shown in Fig. 4. The curve shows the allowable initial momenta $\Psi'(0)$ for the eigenfunction $\Psi(t)$ that are bounded as $t \to \pm\infty$, versus the shear parameter s. The shaded regions in Fig. 4 represent the allowable initial values for $\Psi'(0)$. The lowest values of $\Psi'(0)$ gives the minimum flow velocity for the vortex core required for the formation of the coherent trapped structure. Both the Figures 3 and 4 consistently support the scaling laws presented by Eqs. (28) and (29). In addition, Fig. 4 shows that the existence of a vortex for small electric fields $\Psi'(0)$ (or flow velocity) requires that $s \geq 0.06$, whereas for large electric fields a vortex is formed for $s \geq 0.02$.

Note that the dipole solutions presented here are different from the Larichev and Reznik's modons.[1] The modon construction uses two different linear functions $F(\varphi - ux)$ in the two different regions, namely, the interior and exterior regions of a modon; thus, the equations determining the modon structure are two linear equations. These two equations are solved separately in the two regions and the solutions from the two regions are matched up to second derivatives at the boundary. However, the construction of the new dipole solutions presented here uses only one single arbitrary function $F(\varphi - ux)$. Therefore the derivatives of the eigenfunction $\varphi = (u/k)\Psi$ are continuous to any order in the whole x-y plane. Furthermore, the equation determining the structure of the dipole is a nonlinear multi-eigenvalue equation. When the parameter S_1 and u are given, one can find multiple eigenfunctions $\varphi_n(x)$ with different amplitudes and derivatives $d\varphi_n(x = 0)/dx$. The derivatives $d\varphi_n(x = 0)/dx$ of eigenfunctions form a banded continuous spectrum as a function of the parameter s =

$S_1/\sqrt{2}(u - v_{d0})$ as shown in Fig. 4.

From the analysis, we conclude that when the magnetic shear parameter $s \ll 0.02$, the effect of magnetic shear on drift waves is small and the coupling between the vorticity and parallel velocity fields is weak. The decoupled vorticity equation becomes the H-M equation and therefore we recover the modon solutions. With the increase of s, the coupling between the two fields becomes important. When $0.02 \leq s \leq \sqrt{2}/2$, the new type of dipole vortex emerges. The new vortices are localized solitary waves. However, when $s > \sqrt{2}/2$, the strong coupling between the drift waves and ion acoustic waves causes strong radiation damping of energy from the vortex cores and thus eliminates the existence of the solitary waves.

Even though the above analysis is based on the 1-D model, it exhibits the main features of the solitary vortex induced by magnetic shear. The 2-D simulations of Eqs. (4) and (5) discussed in the following section show that the principle features of the one-dimensional model are consistent with the simulation. As the shear parameter increases the x-variation of the coherent structure becomes stronger than the y-variation and the one dimensional model becomes more accurate. The 1-D model is adequate qualitative picture, but does not yield quantitative values for the amplitudes.

IV. Numerical Vortex Solution in Inhomogeneous Plasma with Sheared Field

In order to facilitate the numerical solutions of Eqs. (4) and (5), we first expand Eq. (4) according to the ordering in Eq. (7) and consider $v'_{d0} \sim \kappa_T \sim \epsilon_n \sim \epsilon$. Keeping only the terms of order ϵ and ϵ^2, we derive from Eqs. (4) and (5) the reduced dynamical equations

$$\left(\frac{1}{T(x)} - \nabla^2\right)\frac{\partial \varphi}{\partial t} + (v_{d0} + v'_{d0}x - \kappa_T\varphi)\frac{\partial \varphi}{\partial y} - \left[\varphi,\ \nabla^2\varphi\right] = -S(x)\frac{\partial v_{\|}}{\partial y}\ , \tag{30}$$

$$\frac{\partial v_{\|}}{\partial t} + \left[\varphi, v_{\|}\right] = -S(x)\frac{\partial \varphi}{\partial y} + \mu\nabla^2 v_{\|}\ . \tag{31}$$

Here $v'_{d0} = \rho_{s0} dv_d/dx \sim (\rho_{s0}/r_n) v_{d0}$ at the core of the vortex. In writing Eq. (31) we have included a viscous damping term to absorb energy transferred to $|k| \to \infty$.

To solve Eqs. (30) and (31), we use a uniform grid over x and k_y in 85×85 xk_y-space with 3655 complex $\varphi_{x,k_y}(t)$ and $v_{\|x,k_y}(t)$ modes. Since the first term of Eq. (30) depends on x, we leave the equation in x space and use the second order central difference formula for ∂_x^2, which yields a tridiagonal system that is solved for each $\partial_t \varphi(x, k_y, t)$. We use the Ahlberg-Nilson-Walsh algorithm for cyclic tridiagonal systems[10] to reduce the operator $(1/T(x) - \nabla^2)$ to a cyclic tridiagonal matrix. Upon inverting the matrix we obtain $\partial_t \varphi(x, k_y, t)$ for each mode. The nonlinear convolution terms in both the equations are evaluated by first transforming φ and $v_{\|}$ in $k_x k_y$ space to get derivatives of φ and $v_{\|}$, then transforming $\varphi_{\mathbf{k}}$ and $v_{\|\mathbf{k}}$ and their derivatives into xy-space to calculate the convolutions. The results are then transformed back into xk_y-space. Finally we use high order Runge-Kutta time stepping to get $\varphi(x, k_y, t)$ for each mode at each time step. The constants of motion defined in Eqs. (9)-(12) are used to monitor the accuracy of the code. The modon of Larichev and Reznik is taken as the initial perturbation for $\varphi(x, y, t = 0)$, and Eq. (17) with $v_\infty = 0$, for $v_{\|}$. The exponential temperature profile $T(x) = \exp(-c_2 x)$ is used so as to avoid the negative temperature problem that can arise when expanding $T(x)$ as $1 - c_2 x$. For the exponential profile $\kappa_T = -(1/T^2) dT/dx = c_2 \exp(c_2 x)$. Because of periodic boundary condition, we choose the magnetic shear profile as $S(x) = S_m \sin(2\pi x/L_x)$, where $L_x = 20\pi\rho_{s0}$ is the length of periodic simulation box in the x-direction. Typical simulations use an average of 40 minutes CPU time on the CRAY-2 for $\Delta t = 100\, r_n/c_s$ which is about 10 rotations of the vortex core.

In the first case we used $v'_{d0} = c_2 = 0$, $\mu = 0.1$ and $S_m = 0.1$ so that $S_1 \simeq 0.01$ and the effective shear $s \simeq 0.07$, which give the parameter $|u/v_d - 1| = 0.1 \gg S_1$, therefore the radiative damping of the vortex is small and negligible. We start with Larichev and Reznik's modon with $u = 1.1 v_{d0}$ and $r_0 = 6.0\rho_{s0}$, so that the center derivative of the modon

$\varphi'(0) \equiv (\partial\varphi/\partial x)_{x=0} \simeq 6.7$ or $\Psi'(0) \simeq 6.1$ where $t = kx$. We observe that the dipole vortex structure for the φ field stays a long time without much change, and that the $v_{||}$ field, though experiencing some change, still keeps a rather coherent and stable structure in the interior region of the dipole vortex. After a long time, the amplitude of the dipole $\varphi_m \sim 13$, the velocity $u \sim 1.3$, and the center derivative $\varphi'(0)$ slightly increases. Figure 5 shows the streamline of $\varphi(x,y,t) = \text{const.}$ and $v_{||}(x,y,t) = \text{const.}$ at times $tc_s/r_n = tv_{d0}/\rho_{s0} = 0$, 20, 40 and 60.

In the second case, temperature gradients exist. We choose $c_2 = 0.046$, $v'_{d0} = 0$, $S_m = 0.1$, $u = 1.1v_{d0}$ and $\mu = 0.1$. For these values the dipole discussed in the first case can not survive. Figure 6 shows that the dipole separates into monopoles immediately after it starts to travel. This is expected since the c_2 introduces the KdV nonlinear term in Eq. (30) that breaks down the symmetries of Eq. (27) and causes the waves in the region of negative potential to propagate faster as reported in Refs. 6 ($\alpha = -\kappa_T$ in Ref. 6) and 8.

We also did some numerical experiments with $s \sim 1$ or $|u/v_d - 1| \sim S_1$, and found that the dipoles eventually connect to oscillating tails with significantly large amplitudes. In these cases the dipole vortices experience strong damping of energy through the tails.

In all the simulations, we notice that the waves with small amplitudes in the $v_{||}$ field appear to be stationary and that the energy of the $v_{||}$ field tends to go into waves with small scale lengths. The reason for these phenomena is that Eq. (31) does not have a linear wave term like $v_{d0}\partial\varphi/\partial y$ as in Eq. (30); thus linear waves with small amplitude do not propagate. Since Eq. (31) lacks linear dispersion, the nonlinear steeping process cannot be effectively balanced and the waves with small scale lengths tend to grow. Because of this fact, we add a viscous term in Eq. (31) to dissipate the energy transferred to the waves with these small scale lengths.

The results of the simulations show the general consistency with the results of the analysis in the previous section. In particular, the simulations show that the dipole-type vortex

solutions of the drift wave-ion acoustic wave system can exist in a sheared magnetic field when the electron temperature is constant over the vortex. The dipole type vortices are well formed and can last a long time without much damping if $s < 1$ or $|u/v_d - 1| > S_1$ provided the $\kappa_T \to 0$. For finite κ_T we can estimate[6] the life time of the dipole vortex from $t_L \sim 1/\kappa_T \varphi_m k \sim 1/\kappa_T \varphi'(0) k^2$.

V. Summary and Conclusions

Analytical and numerical studies of the effect of magnetic shear on drift wave vortices in inhomogeneous plasmas have been reported. Analytically we have derived a solitary vortex equation that includes the effects of density and temperature gradients and magnetic shear, and we have used a quasi-one-dimensional model to exhibit the main features of solitary vortices in sheared magnetic fields. The analysis shows that in a plasma with constant temperature and drift velocity, the presence of a small magnetic shear will cause the effective potential to change from a non-trapping to a trapping potential, which indicates the possible formation of solitary vortex structures with finite amplitudes. The solutions are shown to have the dipole-type symmetry. However, they are different from the well-known modon vortices, because the derivatives of their eigenfunctions are continuous to any order in the whole plane, also, the center derivative $\varphi'(0)$ and the amplitudes form a banded continuous spectrum.

It is also shown that the presence of the magnetic shear intrinsically causes the solitary drift waves to couple to the ion acoustic waves. Thus the dipole solutions are not monotonically decreasing functions, instead, they have oscillating tails with monotonically decreasing amplitudes connecting to the core of vortices. This behavior is similar to the monopoles induced by the gradient of drift velocity in shearless magnetic fields.[8] The oscillating tails cause radiative damping of vortex energy. The damping is negligible if the amplitude $\varphi_m (\sim \sqrt{2}\, u^2 k / S_1)$ of the dipole structure satisfies $\varphi_m > \sqrt{2} u / k$. For a weak effect

of magnetic shear, this condition is consistent with that for the Larichev-Reznik's modon. However, for shear above a small threshold value $s > s_c \approx 0.02$ as given in Fig. 4, we find that the nonlinearity of the $v_{||}$ induced by the shear and vorticity equations combine to produce a nonlinear restoring force proportional to $(S_1^2/2u^4)\varphi^3$ which gives the new dipole vortex structures when $s > 0.02$ or $S_1 > 0.03|u/v_d - 1|$. The nonlinear structures in the weakly sheared field greatly reduce the shear radiation expected in the linear drift wave-ion acoustic wave theory.

The numerical simulations performed in 2-D with the coupled vorticity and parallel mass flow equations consistently support the analysis. The simulations show that for a plasma with constant temperature and drift velocity in a magnetic field with small shear, the well-formed dipole vortices are stable and can last a long time without much damping when $|(u/v_d) - 1| > S_1$. However with the presence of a small temperature gradient, the dipole vortices become structurally unstable and are rapidly separated into monopole vortices, which is consistent with our previous studies[6,8] on the effect of finite inhomogeneities across the core of the vortex. Therefore we conclude that with constant temperature and drift velocity, the coherent structures of drift wave plasmas behave like dipole vortices in either shearless or sheared magnetic fields. But when the gradients of temperature and drift velocity exist, the solitary coherent structures take the form of monopole vortex structures rather than dipole structures.

Acknowledgments

The authors thank V.E. Zakharov for useful conversations. The work was supported by the U.S. Department of Energy contract no. DE-FG05-80ET-53088.

Appendix: Noncanonical Hamiltonian Structure

The vorticity equation (4) and the parallel momentum equation (5) with the Boltzmann density distribution n given in Eq. (6) can be rewritten to order ϵ and ϵ^2 for $\partial/\partial z = 0$ as follows:

$$\frac{\partial q}{\partial t} + [\varphi\ ,\ q] = S(x)\frac{\partial v_{||}}{\partial y} \tag{32}$$

$$\frac{\partial v_{||}}{\partial t} + \left[\varphi\ ,\ v_{||}\right] = -S(x)\frac{\partial \varphi}{\partial y} \tag{33}$$

where the potential vorticity $q(x,y,t) = \nabla^2\varphi - \varphi/T(x) - \ell n(n_0(x))$.

The Hamiltonian is, from Eq. (11),

$$\begin{aligned} H(q, v_{||}) &= \frac{1}{2}\int\left[\frac{\varphi^2}{T(x)} + (\nabla\varphi)^2 + v_{||}^2\right] dxdy \\ &= \frac{1}{2}\int\left(-q\varphi - \varphi\ell n_0 + v_{||}^2\right) dxdy\ , \end{aligned} \tag{34}$$

where surface terms are neglected. Upon variation of H

$$\delta H = \int\left(-\varphi\delta q + v_{||}\delta v_{||}\right) dxdy$$

and we obtain the functional derivative

$$\frac{\delta H}{\delta q} = -\varphi\ ; \qquad \frac{\delta H}{\delta v_{||}} = v_{||}\ . \tag{35}$$

Equations (32) and (33) can be written in Hamiltonian form,

$$\frac{\partial q}{\partial t} = \{q, H\}\ , \tag{36}$$

$$\frac{\partial v_{||}}{\partial t} = \left\{v_{||}, H\right\}\ , \tag{37}$$

where the noncanonical Poisson bracket $\{F\,,\ G\}$ is defined as

$$\{F\,,\ G\} = \int \left\{ q \left[\frac{\delta F}{\delta q}\,,\ \frac{\delta G}{\delta q} \right] + \left(v_{\|} - \sigma(x) \right) \left(\left[\frac{\delta F}{\delta v_{\|}}\,,\ \frac{\delta G}{\delta q} \right] + \left[\frac{\delta F}{\delta q}\,,\ \frac{\delta G}{\delta v_{\|}} \right] \right) \right\} dxdy\ , \quad (38)$$

where $\sigma(x) = \int^x S(x')dx'$.

It is easily shown that the Poisson bracket given by Eq. (38) is antisymmetric,

$$\{F, G\} = -\{G, F\}\ ,$$

and one can prove it satisfies Jacobi's identity,

$$\{E, \{F, G\}\} + \{F, \{G, E\}\} + \{G, \{E, F\}\} = 0\ .$$

(A proof for essentially the same bracket can be found in Ref. 11.)

The Casimir invariants C of the Poisson bracket are defined by

$$\{C, D\} = 0\ , \quad (39)$$

where D is an arbitrary function. Substituting Eq. (39) into Eq. (38), we obtain

$$\{C, D\} = \int \left\{ q \left[\frac{\delta C}{\delta q}\,,\ \frac{\delta D}{\delta q} \right] + \left(v_{\|} - \sigma(x) \right) \left(\left[\frac{\delta C}{\delta v_{\|}}\,,\ \frac{\delta D}{\delta q} \right] + \left[\frac{\delta C}{\delta q}\,,\ \frac{\delta D}{\delta v_{\|}} \right] \right) \right\} dxdy = 0\ . \quad (40)$$

Using the identity,

$$\int f[g, h]dxdy = \int h[f, g]dxdy\ , \quad (41)$$

we can rewrite Eq. (40) as

$$\int \left(\frac{\delta D}{\delta q} \left[q\,,\ \frac{\delta C}{\delta q} \right] + \frac{\delta D}{\delta q} \left[\left(v_{\|} - \sigma(x) \right)\,,\ \frac{\delta C}{\delta v_{\|}} \right] + \frac{\delta D}{\delta v_{\|}} \left[\left(v_{\|} - \sigma(x) \right)\,,\ \frac{\delta C}{\delta q} \right] \right) dxdy = 0\ . \quad (42)$$

Since D is arbitrary its coefficient must vanish, and we can find two independent Casimirs, from Eq. (42)

$$C_1 = \int f[v_{\|} - \sigma(x)]dxdy\ ,$$

$$C_2 = \int qg[v_{\|} - \sigma(x)]dxdy\ ,$$

where f and g are arbitrary functions of their arguments. When $\partial/\partial z \neq 0$, it can be easily shown that

$$\hat{C}_1 = \int q dx dy dz \ ,$$

$$\hat{C}_2 = \int \left(v_{||} - \sigma(x) \right) dx dy dz \ ,$$

$$\hat{C}_3 = \int q \left(v_{||} - \sigma(x) \right) dx dy dz \ ,$$

survive.

References

1. V.D. Larichev and G.M. Reznik, Oceanology **16**, 547 (1976).

2. A. Hasegawa and K. Mima, Phys. Fluids **21** 87 (1978); A. Hasegawa, C.G. Maclennan, and Y. Kodama, Phys. Fluids **22**, 2122 (1979).

3. V.I. Petviashvili, Fiz. Plazmy **3**, 270 (1977) [Sov. J. Plasma Phys. **3**, 150 (1977)].

4. W. Horton, Phys. Fluids B **1**, 424 (1989).

5. M. Makino, T. Kamimura, and T. Taniuti J. Phys. Soc. Jpn. **50**, 908 (1981).

6. X. Su, W. Horton, P.J. Morrison, and V.P. Pavlenko, "Effect of Scalar Nonlinearity on the Dipole Vortex Solution", U. of Texas at Austin, IFSR# 328, (1988).

7. K.H. Spatschek, E.W. Laedlke, Chr. Marquardt, S. Musher, H. Wenk, Phys. Rev. Lett. **64**, 3027 (1990).

8. X.N. Su, W. Horton and P.J. Morrison, Phys. Fluids B **3**, 921 (1991).

9. J.D. Meiss and W. Horton, Phys. Fluids **26**, 990 (1983).

10. C. Temperton, J. Comp. Phys. **19**, 317 (1975).

11. P.J. Morrison and R.D. Hazeltine, Phys. Fluids **27**, 886 (1984).

Figure Captions

1. Evolution of effective potential $V_{\text{eff}}(\Psi, t)$ with the "time" t that corresponds to the distance kx from the shear reversal point.

2. Evolution of the separatrix in phase space corresponding to the effective potential $V_{\text{eff}}(\Psi, t)$.

3. Nonlinear eigenfunction for $s = 0.06$ and $d\Psi(t = 0)/dt = 13.58$ showing the dipole type vortex and wave solutions in the case without temperature and drift velocity gradients.

4. Spectrum of critical $d\Psi(t = 0)/dt$ versus the effective shear s from 0 to 0.1, showing the allowable initial "momenta" $d\Psi(t = 0)/dt$ in the range of 0 — 50 for the eigenfunction $\Psi(t)$ to be bounded as $t \to \pm\infty$. The shaded regions represent the allowable initial values for $d\Psi(t = 0)/dt$.

5. Contour plots of the electrostatic potential $\varphi(x, y, t)$ and parallel velocity $v_{\|}(x, y, t)$ of Eqs. (30) and (31) with temperature gradient $\kappa_T = 0$, drift velocity gradient $v'_{d0} = 0$ and magnetic shear parameter $S_m = 0.1 (s \simeq 0.07)$. The dipole-type vortex does not change much for a long time.

6. Contour plots of the electrostatic potential $\varphi(x, y, t)$ and parallel velocity $v_{\|}(x, y, t)$ of Eqs. (30) and (31) with temperature gradient parameter $c_2 = 0.046$, drift velocity gradient $v'_{d0} = 0$ and magnetic shear parameter $S_m = 0.1$. The dipole-type vortex breaks up after a short time.

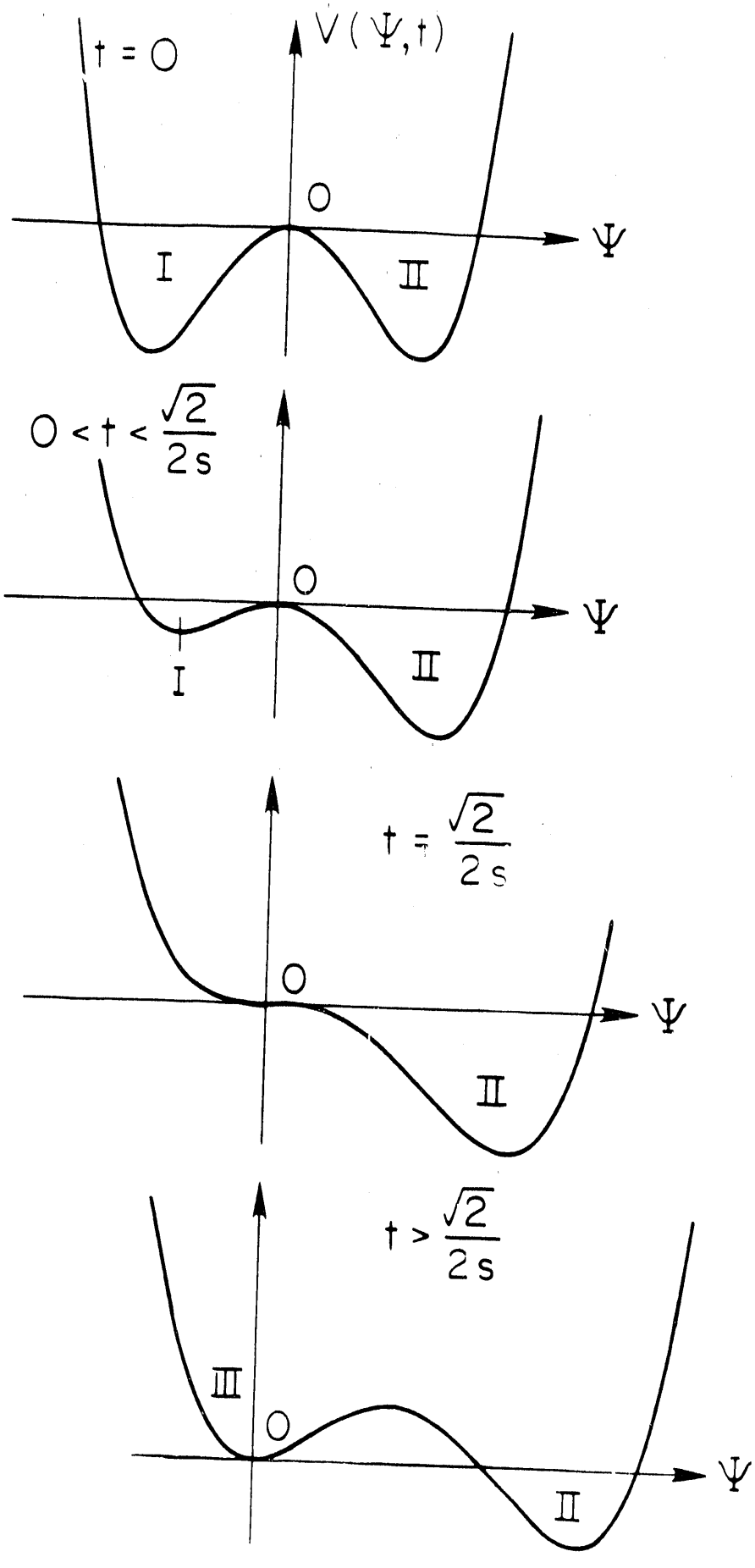

Fig. 1

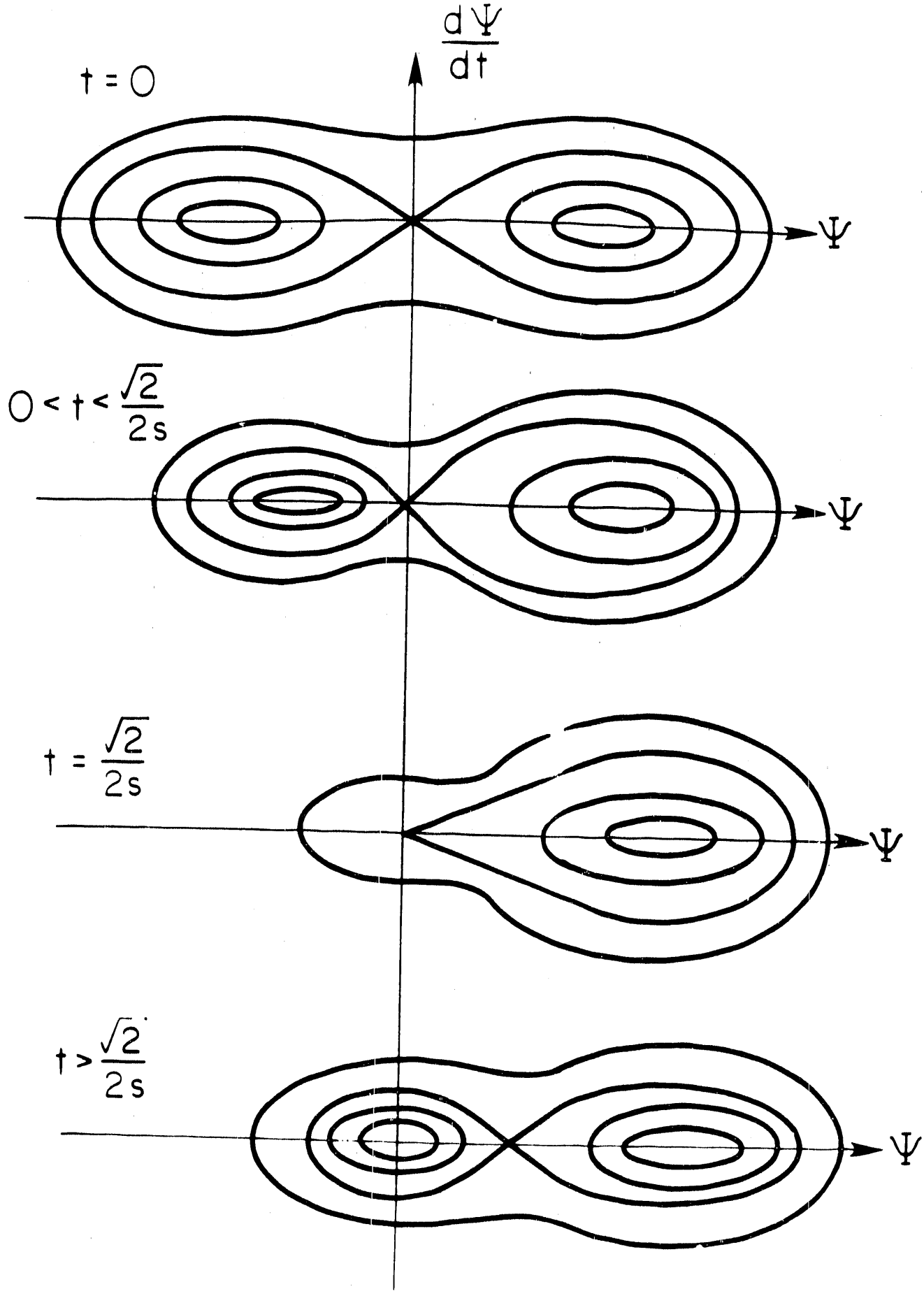
$\frac{d\Psi}{dt}$
$t = 0$
Ψ
$0 < t < \frac{\sqrt{2}}{2s}$
Ψ
$t = \frac{\sqrt{2}}{2s}$
Ψ
$t > \frac{\sqrt{2}}{2s}$
Ψ

Fig. 2

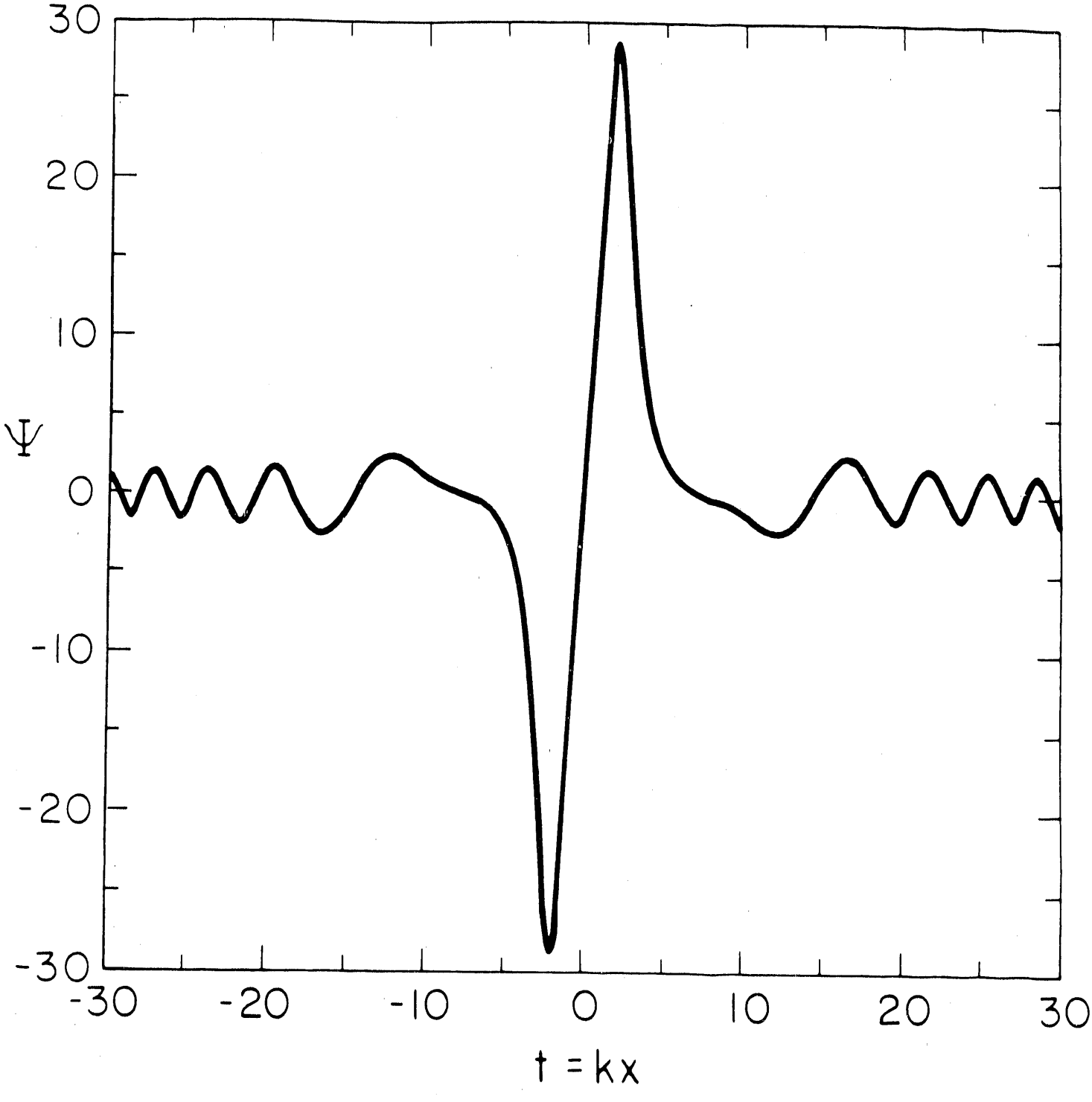

Fig. 3

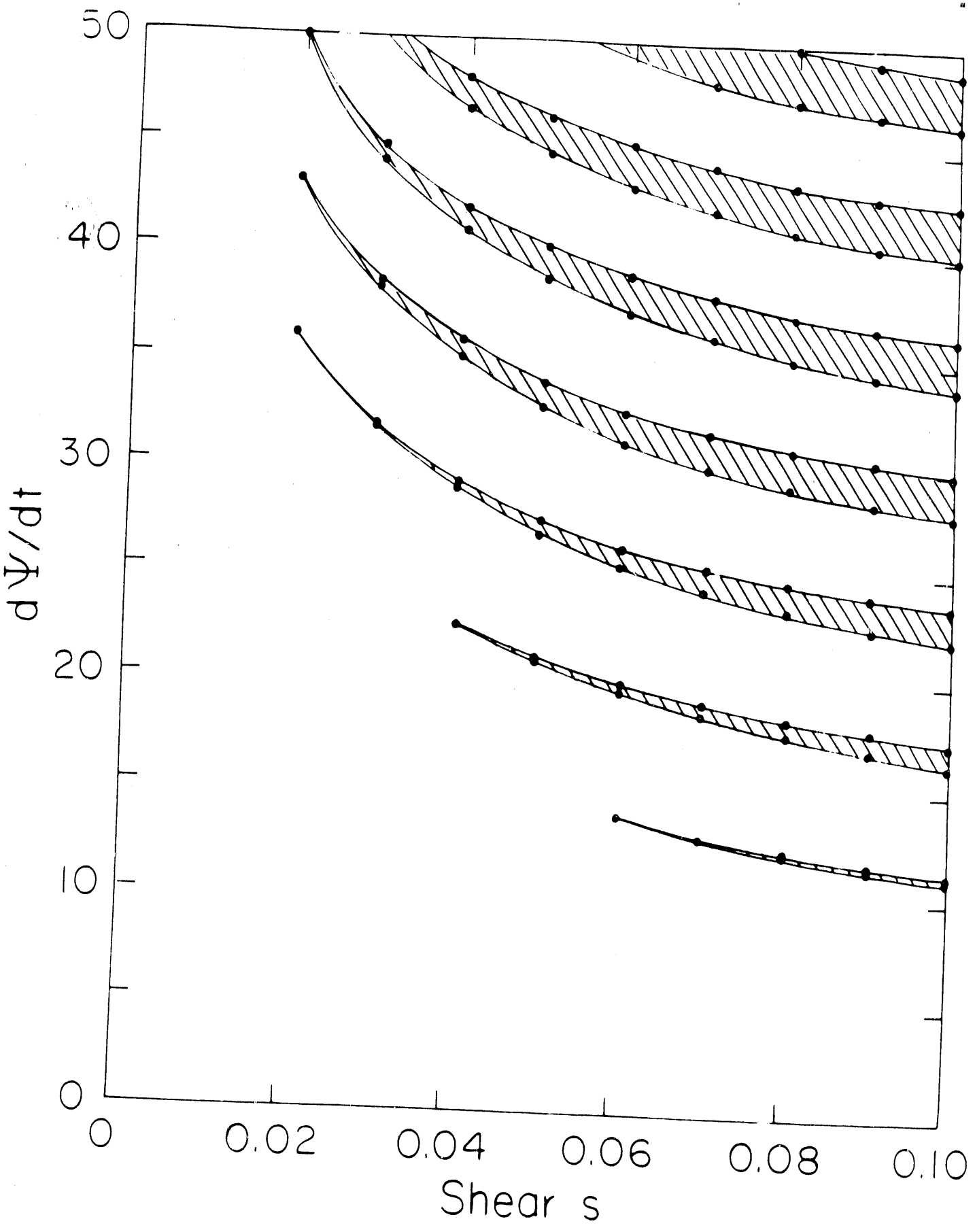

Fig. 4

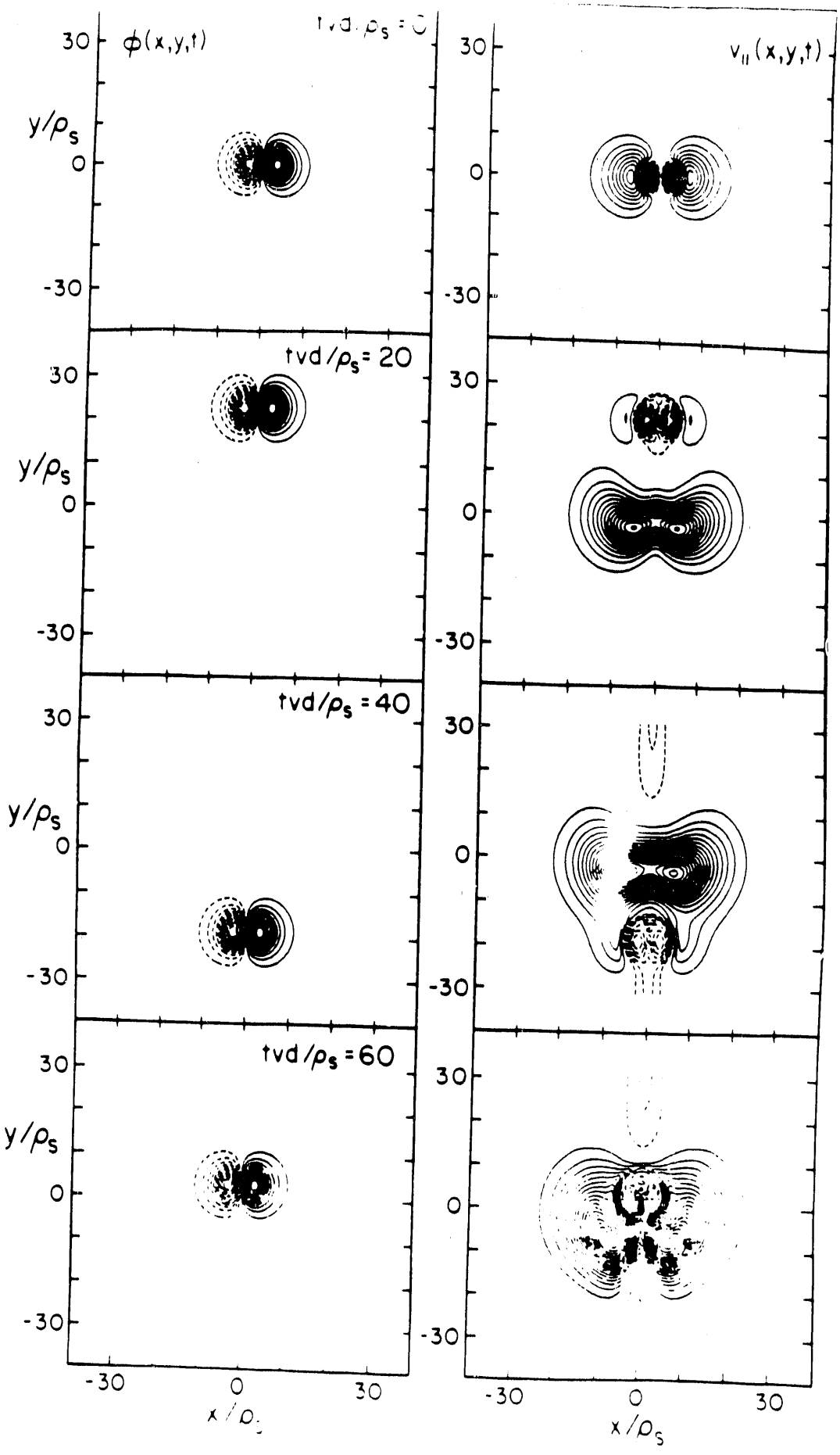
$\phi(x,y,t)$
$v_{\parallel}(x,y,t)$
tvd/ρ_s = 0
tvd/ρ_s = 20
tvd/ρ_s = 40
tvd/ρ_s = 60
30
0
-30
y/ρ_s
x/ρ_s

Fig. 5

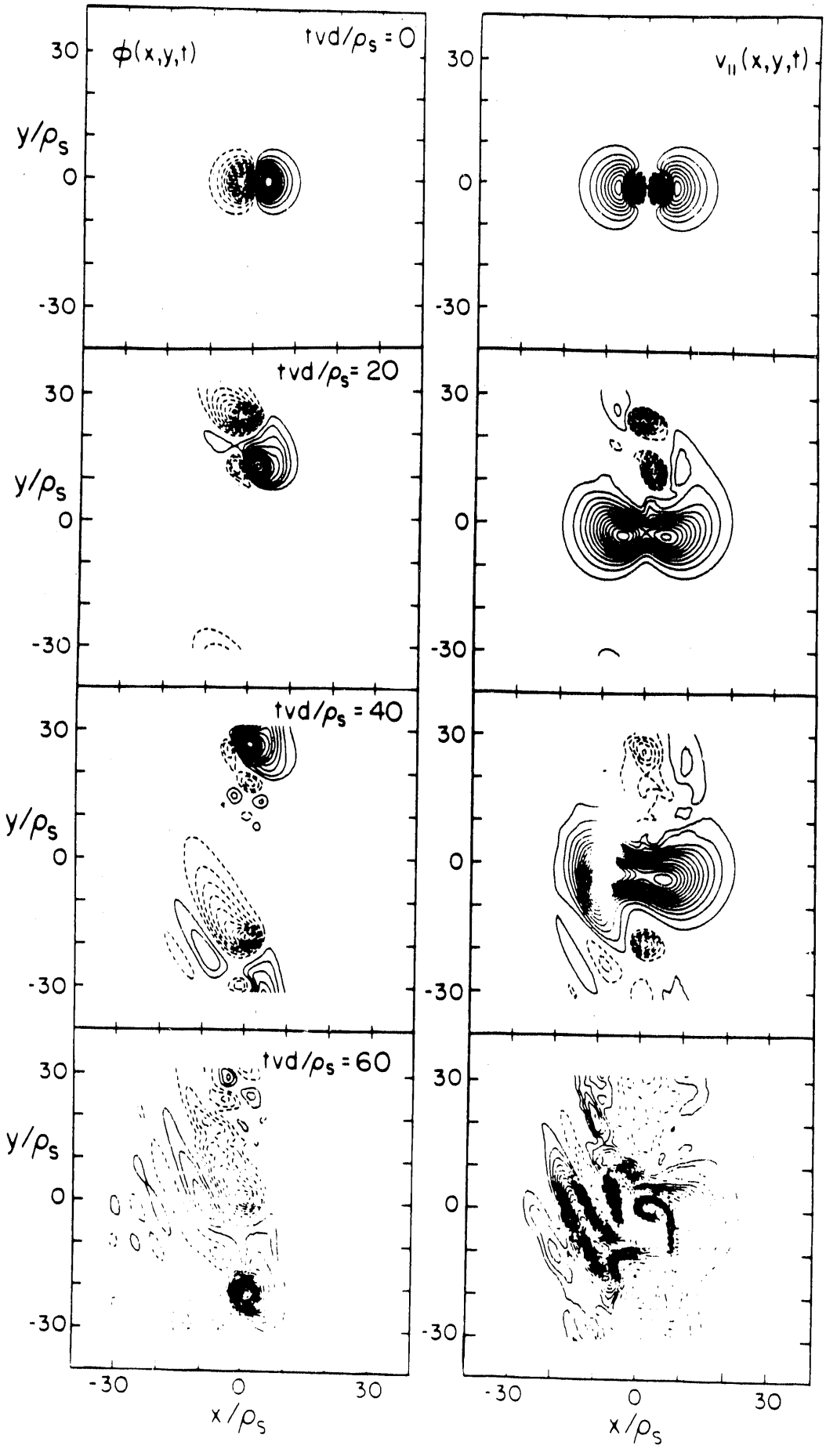
$\phi(x,y,t)$
$tvd/\rho_s = 0$
$v_{\parallel}(x,y,t)$
$tvd/\rho_s = 20$
$tvd/\rho_s = 40$
$tvd/\rho_s = 60$
30
0
-30
y/ρ_s
x/ρ_s

Fig. 6

END

DATE
FILMED
3/3/92